PHOENIX models (Section 3.4.2. The maximum difference between the significance of these slopes for all of three stellar models is negligible, which suggests that any importance of stellar models vanishes somewhat when looking at the ratios. Nevertheless, we keep the results from the PHOENIX models (Section 3.4.2).

3.C Comparing effective temperatures with Schwartz & Cowan (2015)

Schwartz & Cowan (2015) measure the slope of the effective dayside temperature against the irradiation temperature. They note that their slope 0.87 ± 0.05 is significantly steeper than equilibrium temperature predictions (0.71), and that this increasing deviation could lower redistribution efficiencies in the hottest planets. We recreate their results with our expanded survey. We follow their method for calculating the effective temperature, which is the weighted mean of the brightness temperatures, and thus we call it $T_{\rm eff} = (T_{b_{3.6}}/\sigma^2_{3.6} + T_{b_{4.5}}/\sigma^2_{4.5})/2$. We then fit the resulting trends with an ODR (see Section 3.A.1. However, first we test their method of brightness temperature calculation of inverting the Planck function and using a blackbody for the star. Then we test our method using a stellar model and fully integrating the Planck function.

Table 3.1 presents the results for weighted mean effective temperature using the PHOENIX model calculations of the brightness temperatures. We find a slope of 0.80±0.03, which is both consistent to within 1.5σ with equilibrium temperature and with the 0.87 ± 0.05 slope of Schwartz & Cowan (2015). This does not support the findings of Schwartz & Cowan (2015) that the effective temperature is significantly steeper than the equilibrium temperature. However, using the brightness temperatures calculated without integration over the bandpass and with blackbodies for the star we are able to retrieve a slope of 0.85 ± 0.05, which is in statistical agreement (0.3σ) with their trend.

Additionally, Table 3.1 demonstrates that the deviation of the effective temperature ($T_{\rm eff}$) slope from the equilibrium temperature slope (0.71) is driven by the steeper slope at 4.5 μm, i.e. the slope measured at 4.5 μm is steeper than the slope at 3.6 μm for all stellar models. As mentioned above, typically, the effective temperature is calculated as the weighted average of the brightness temperatures over the spectral energy distribution. In this analysis, we only have two bandpasses and one of them has a strong molecular feature (CO at 4.5 μm) which could strongly bias the results. We therefore suggest that the effective temperature is better approximated by the 3.6 μm brightness temperature alone, since 3.6 μm probes closer to the continuum. Figure 3.8 presents the results for approximating the effective temperature with the 3.6 μm brightness temperature using the PHOENIX model calculations of the brightness temperatures. We find a slope of 0.76±0.05, which is consistent with equilibrium temperature (1σ) and inconsistent with the strong slope of 0.87 ± 0.05 of Schwartz & Cowan (2015).

Regardless of whether we take the effective temperature as the weighted mean of the two brightness temperatures or as the 3.6 μm brightness temperature alone, we do not see a that

the effective temperature slope is statistically significantly larger than that of the equilibrium temperature. These findings do not support the findings presented in Schwartz & Cowan (2015) as we do not find that the effective temperature trend with irradiation temperature increases disproportionately. This means that we do not think the effective temperature calculated in this way tells us anything about the redistribution in the hottest planets. However, since we are able to retrieve the results of Schwartz & Cowan (2015) using blackbodies and the mean of the brightness temperatures, we conclude that the discrepancy is a result of careful use of stellar models and integration over the bandpasses and not due to differences in the samples.

On the other hand, in Figure 3.3, we find that the 4.5 μm brightness temperature is deviating from equilibrium, likely due to the strong CO opacity appearing in emission. This does support the hypothesis that these hottest planets are exhibiting different behaviors than their cooler counterparts, but it is not expected to be captured in the effective temperatures since the weighted mean of the two brightness temperatures is likely muting this deviation.[2]

3.D KELT-9b Eclipse: the hottest of the UHJs

A question arises of whether the trends presented in Section 3.5 hold at even higher temperatures. To test this we include the 4.5 μm eclipse depth of the hottest of the UHJs, KELT-9b (Gaudi et al. 2017). Significantly hotter than any other ultra-hot Jupiter, KELT-9b is the hottest gas giant planet known. A 1.48-day orbital period around its A-type host star of 10170K makes it the most highly irradiated planet with an equilibrium temperature of 4050K (Gaudi et al. 2017). At these temperatures, the planet itself is similar to a K4 star; its atmosphere is subject to molecular dissociation, leaving behind atomic metals such as iron and titanium (Hoeijmakers et al. 2018, 2019).

We analyse two 4.5 μm eclipses of KELT-9b. The data were taken from the phase curve survey, program ID 14059 lead by PI J Bean. We extracted the two secondary eclipses from the available phase curves. The analysis from raw data to eclipse depth values was done using our custom pipeline described in Baxter et al. (in prep.). In summary, we allow for different background correction methods, different centroiding methods, and different aperture radii to find the combination that gives the lowest χ^2. We correct for the strong *Spitzer* systematics using Pixel Level Decorrelation (Deming et al. 2015) and perform a full MCMC analysis using Batman (Kreidberg 2015) to fit for the eclipse parameters on the best photometric lightcurve. The raw photometry, the corrected lightcurves, and one of our statistical tests (RMS vs binsize, which characterizes how well we correct red noise) are presented in Figure 3.9. The two eclipse depths (Fp/Fs) are calculated to be 2793 ± 44 (ppm) and 2809 ± 48 (ppm) for AORs r67667712 and r67667968, respectively. The eclipse depth used in the analysis is the mean of these two values 2801 ± 33 (ppm). This eclipse depth is used to calculate the brightness temperatures shown in Figure 3.3.

[2]This section has been edited from the original publication.

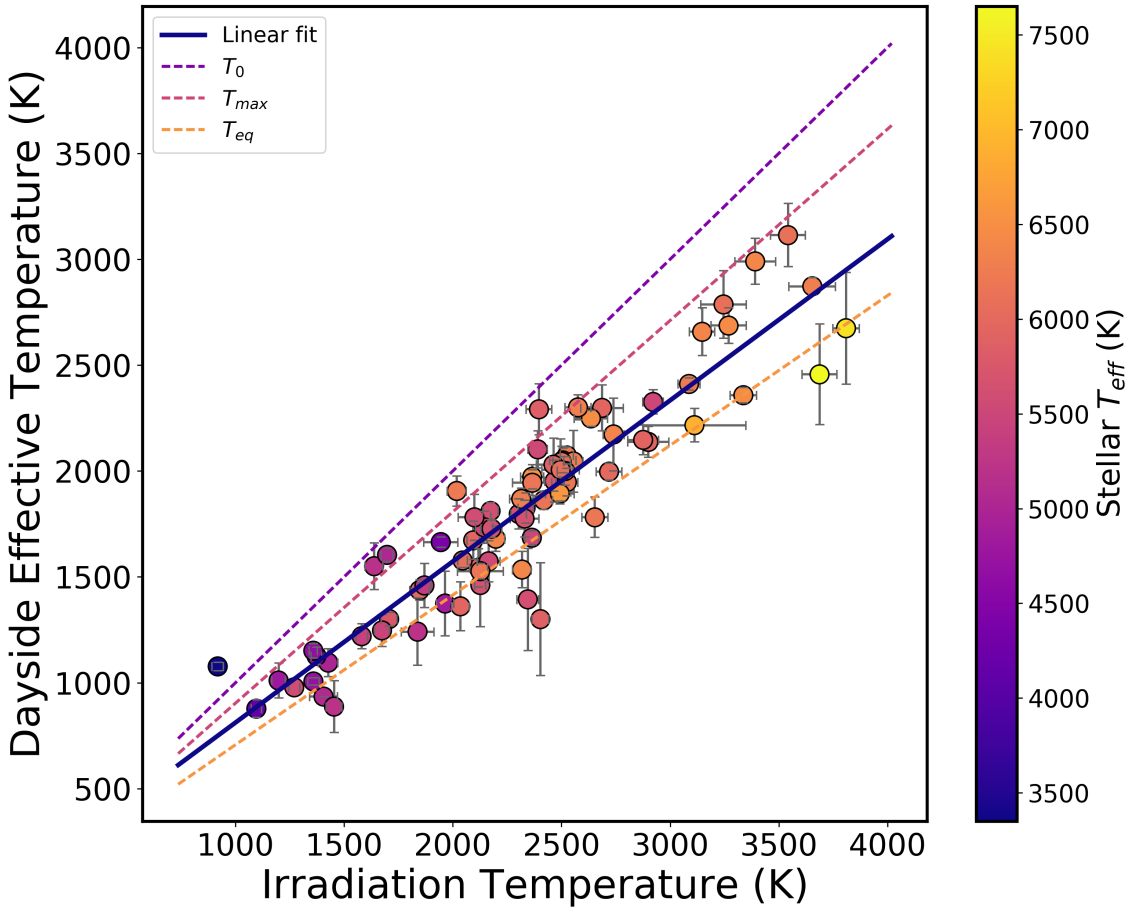

Fig. 3.8: Dayside effective temperature ($T_{\rm eff}$) vs the theoretical irradiation temperature (T_{eq}) with zero albedo and full redistribution, similar to Schwartz & Cowan (2015), but with 28 more planets. We also plot the expected irradiation temperature (T_0), the equilibrium temperature with zero albedo (T_{eq}), and the maximum dayside temperature (T_{max}). The color scale is the effective temperature of the host star in Kelvin.

Our results disagree with the 4.5 μm eclipse depths presented in Mansfield et al. (2020) by 4.6σ. This significant difference is likely not due to any problems with the systematic correction algorithm, but is rather a result of the choice of baseline between eclipse and phase curve observations. Eclipse-only observations ignore phase variations, and can thus underestimate eclipse depths when the real phase variations are concave over the secondary eclipse (e.g., Bell et al. 2019). Since the large phase amplitude (0.601) presented in Mansfield et al. (2020) clearly demonstrates a concave phase variation around the ellipse, this is likely the cause of the discrepancy between the two sets of data analyses. However, since we do not see any trend with the phase curve offsets between the two *Spitzer* bandpasses (discussed in Section 3.5.4.1) we expect that any underestimation of the eclipse depth will apply to both 3.6 μm and 4.5 μm, and thus the deviation from the blackbody will be largely unaffected. Nevertheless, such an effect could be relevant for higher precision measurements with the